Article

Improvement of Mechanical Properties and Condensation Behavior for Alkali-Activated Materials by Sodium Silicate

Mingjing Li [1], Guodong Huang [1,2,3,*], Yi Cui [1], Bo Wang [1], Shuwei Zhang [1], Qi Wang [1] and Jiacheng Feng [1]

1   School of Civil Engineering and Construction, Anhui University of Science and Technology, Huainan 232001, China; lmj201007@126.com (M.L.); yicui@aust.edu.cn (Y.C.); bowang@aust.edu.cn (B.W.); swzhang@aust.edu.cn (S.Z.); qiwang@aust.edu.cn (Q.W.); jcfeng@aust.edu.cn (J.F.)
2   Hefei Comprehensive National Science Center, Institute of Energy, Hefei 230031, China
3   Institute of Environment-Friendly Materials and Occupational Health, Anhui University of Science and Technology, Wuhu 241003, China
*   Correspondence: gdhuang@aust.edu.cn

Abstract: To further enhance the compressive strength of alkali-activated materials and reveal their condensation behavior, the reactivity of alkali-activated slag materials was enhanced through the addition of different kinds and proportions of sodium silicate. The mechanical properties of the specimens were observed regularly and the condensation behavior was further analyzed. The results showed that both solid and liquid sodium silicate could significantly improve the compressive strength. The maximum increase in compressive strength was 123.7%, while the initial and final setting times were significantly shortened to 9 min. When solid sodium silicate content increased from 5% to 15%, the compressive strength first increased to 34.6 MPa and then decreased to 28.6 MPa, indicating that 10% was the optimum solid sodium silicate content. The large amount of crystallized solid sodium silicate in the specimen led to the decrease in mechanical properties. When liquid sodium silicate content increased from 5% to 15%, the compressive strength first increased to 52.8 MPa and then tended to be stable, implying that 10% was the optimum content. This shows that its reinforcement effect has a maximum limit. The activation effect of liquid sodium silicate was better than that of solid.

Keywords: alkali activation; sodium silicate; slag; compressive strength; initial setting; final setting

1. Introduction

Alkali-activated materials are prepared using industrial solid wastes containing silicate or aluminosilicate as raw materials under strong alkali excitation to establish new energy-saving and environmental protection building materials with high strength [1,2]. Research shows that alkali-activated materials not only have the mechanical characteristics of early strength and high strength, but also have lower permeability than cement-based materials in terms of durability [3]. However, the selection of the appropriate activator is the most critical factor for ensuring that alkali-activated materials can achieve excellent mechanical properties and durability [4]. This is because the activator can establish a strong alkaline excitation environment, promote the depolymerization of active substances such as calcium, silicon, and aluminum in raw materials, form new polymerization products after repolymerization, and provide excellent mechanical properties and durability [5].

Relevant experts have conducted in-depth research on the performance of various alkali activators. Prinya Chindaprasirt studied the effects of different concentrations of sodium hydroxide solution on the setting behavior, compressive strength, and electrical properties of high calcium fly ash geopolymer pastes [6]. The results showed that the setting time and compressive strength of the polymer increased significantly with the increase in concentration of sodium hydroxide solution. Murat TuYan studied the effects of activator

concentration and curing conditions on the consistency and strength of geopolymer composites based on waste clay brick powder [7]. The results showed that the optimum alkali activator concentration corresponded to (SiO_2/Na_2O) ratio of 1.6 and Na_2O content of 10% by weight of the binder. A maximum compressive strength of 36.2 MPa was achieved by curing at 90 °C and 40% RH for 5 days. John L. Provis and Susan A. Bernal [8,9] studied the effect of binder content on the performance of alkali slag concrete. They found that with the increase in slag content, the compressive strength, permeability, carbonation resistance, and durability were significantly improved. Although the above research has significantly improved the mechanical properties and durability of alkali-activated materials [10,11], it is necessary to further enhance their mechanical properties to realize wide application in construction engineering and completely replace cement-based materials [12]. Therefore, the mechanical properties of alkali-activated materials need to be further improved in different ways.

With the advance in research, scholars found that the addition of sodium silicate can further improve the properties of alkali-activated materials [13,14]. However, the improvement effect of sodium silicate on the properties of alkali-activated materials is limited, and the mechanism by which sodium silicate participates in the reaction and its influence on the transformation of polymerization are not clear. Therefore, to fully exploit the reinforcing effect of sodium silicate on alkali-activated materials and further improve its performance advantages, it is still necessary to enhance the reaction activity of alkali-activated materials, improve their mechanical properties and durability, and ensure their reliability. Hence, more in-depth research on the excitation properties of activators is required to realize the application of alkali-activated materials in practical engineering.

In this paper, different kinds and amounts of sodium silicate were added to fully stimulate the polymerization activity of slag, and the mechanical properties and setting changes of specimens were observed regularly. X-ray diffraction (XRD) and optical microscopy were also used to deeply analyze the influence of sodium silicate on the micro crystal formation, transformation behavior, and microstructure of alkali-activated slag specimens. These findings can help further improve the preparation of high-performance slag alkali-activated materials.

2. Experimental Contents and Methods

2.1. Experimental Materials and Mix Proportion

2.1.1. Experimental Materials

S95 grade granulated blast furnace slag (Xiangtai Mineral Products Co., Ltd., Shijiazhuang, China) was used for the preparation of alkali-activated specimens. Its performance met the standard of granulated blast furnace slag powder used for cement, mortar and concrete (GB/T 18046-2017) [15]. The surface area of slag was 421 m^2/kg. The chemical composition of slag obtained from X-ray fluorescence spectroscopic analysis (XRF, AXS, Brooke, Germany) is shown in Table 1. These data were obtained from the analysis and testing center of Anhui University of Science and Technology. Sodium hydroxide and sodium silicate were used as activators. Sodium hydroxide was of analytical grade with purity greater than 99.5%. Sodium hydroxide was first dissolved into the test water, and then the alkali excitation material was mixed; the specific mixing amounts and mixing method are detailed in Sections 2.1.2 and 2.2.1 (mix proportion and specimen preparation). Two types of sodium silicate were used: solid and liquid. Solid sodium silicate (SSS, Yatai United Chemical Co., Ltd., Wuxi, China, $Na_2SiO_3 \cdot 9H_2O$) was of analytical grade with purity greater than 99.5%. The liquid sodium silicate (LSS, Yatai United Chemical Co., Ltd., Wuxi, China) used in this work was industrial grade, with purity greater than 95%, and the composition of Na_2O, SiO_2, and H_2O was 9.66%, 25.25%, and 65.03% of the total mass, respectively. Standard sand was used for the experiment and its fineness modulus was 2.8. The test water was tap water.

Table 1. Chemical composition of slag %.

Raw Material	SiO$_2$	Al$_2$O$_3$	Fe$_x$O$_y$	CaO	MgO	Na$_2$O	K$_2$O	Others	Loss
Slag	38.42	16.34	0.84	35.78	2.14	1.26	0.67	1.82	0.93

2.1.2. Experimental Mix Proportion

The mix proportions of the alkali-activated slag specimens for compressive strength and setting time tests are shown in Table 2. The compressive strength experiment adopted the mortar specimen, and the liquid–solid ratio was 0.5. The setting time test adopted the paste specimen, and the liquid–solid ratio was 0.3 (requirement of normal consistency). This paper mainly studies the effect of sodium silicate on the mechanical properties and coagulation behavior of alkali-activated materials. Therefore, the content of sodium hydroxide was kept at 20 g, which achieved good activation effect according to previous studies [3,5,13]. Specimen X-1 was only activated by sodium hydroxide without sodium silicate as the experimental control group. Specimens X-2 to X-6 were activated by both sodium hydroxide and SSS. The content of SSS was gradually increased to test the effect of SSS on compressive strength and condensation behavior. Specimens X-7 to X-11 were activated by sodium hydroxide and LSS; the content of LSS was gradually increased to test the effect of LSS on compressive strength and condensation behavior. The excitation effects with solid and LSS were compared and analyzed.

Table 2. Mix proportion of samples/g.

	Slag	Solid Sodium Silicate	Liquid Sodium Silicate	Sodium Hydroxide	Paste/Mortar Water Consumption	Paste/Mortar Liquid-Solid Ratio	Sand
X-1	450	0	0	20	135/225	0.3/0.5	1350
X-2	450	22.5 (5%)	0	20	135/225	0.3/0.5	1350
X-3	450	33.75 (7.5%)	0	20	135/225	0.3/0.5	1350
X-4	450	45 (10%)	0	20	135/225	0.3/0.5	1350
X-5	450	56.25 (12.5%)	0	20	135/225	0.3/0.5	1350
X-6	450	67.5 (15%)	0	20	135/150	0.3/0.5	1350
X-7	450	0	65 (5%)	20	93/183	0.3/0.5	1350
X-8	450	0	96 (7.5%)	20	73/163	0.3/0.5	1350
X-9	450	0	128 (10%)	20	52/142	0.3/0.5	1350
X-10	450	0	160 (12.5%)	20	31/121	0.3/0.5	1350
X-11	450	0	193 (15%)	20	10/100	0.3/0.5	1350

Note: in the experiment, the content of solid substance in liquid sodium silicate was consistent with the content of solid sodium silicate. For example, in X-7, the content of solid substance in liquid sodium silicate was 65 × 0.35% = 22.75 g.

2.2. Preparation and Curing of Samples

2.2.1. Preparation Method

Different methods were used to prepare specimens with different forms of sodium silicate. When preparing specimen X-6 (with SSS), sodium hydroxide was first dissolved into test water, and then slag and SSS were mixed evenly. Then, standard sand and sodium hydroxide solution were added. The mixture was stirred slowly for 30 s, then stirred quickly for 60 s, and finally pouted into a 40 mm × 40 mm × 160 mm mold. To prepare specimen X-11 (with LSS), sodium hydroxide was first dissolved into the test water. Then, slag was placed in the mixing pot and sodium hydroxide solution was added. The mixture was stirred slowly for 30 s, and then LSS and standard sand were added. The mixture was stirred quickly for 60 s, and finally poured into the same mold.

2.2.2. Curing Method

After the specimen was prepared, it was placed in the curing box (SHBY-40B type, Honghao Construction Equipment Co., Ltd., Cangzhou, China). Then, the mold was

removed immediately after curing for 24 h. The specimen was kept in the curing box until it reached the experimental design age. The temperature of the curing box was kept at $20 \pm 2\ °C$ and the humidity was greater than 95%.

2.3. Experimental Contents and Methods

2.3.1. Compressive Strength Test

The test adopted DYE-300S cement mortar pressure tester (Lukejian Test Instrument Co., Ltd., Cangzhou, China). The measurement was carried out according to the standard of Method of testing cements: determination of strength (ISO method, GB/T 17671-2021) [16]. The compressive strength of the specimens cured for 3 days, 28 days, and 60 days was measured. The experimental results were taken as the average value of six measurements.

2.3.2. Determination of Setting Time

The setting time experiment was carried out by using the standard Vicat instrument (Xingjian Instrument Equipment Co., Ltd., Cangzhou, China) and adhered to the test methods for water requirement of normal consistency, setting time, and soundness of the Portland cement (GB/T 1346-2011) [17]. The purpose of this test was to evaluate the effect of sodium silicate on the setting behavior of alkali-activated slag specimens.

2.3.3. XRD Analysis

SmartLab SE intelligent X-ray diffractometer (RIGAKU, Tokyo, Japan) was used to analyze the mineral crystal composition in alkali-activated specimens X-1, X-2, X-4, X-7, X-9, and X-11, after curing for 28 days. This test evaluated the effect of sodium silicate on the polymerization reaction characteristics and the formation and variation of mineral crystals in alkali-activated slag specimens.

2.3.4. Optical Microscope Analysis

OST-AF 200 HD video microscope produced by Oerster Optical Instruments Co., Ltd. (Suzhou, China) was used to analyze the microstructure of alkali-activated paste specimens X-1, X-4 and X-6 cured for 28 days (magnification: 200 times), and to assess the improvement effect of sodium silicate on the microstructure.

3. Experimental Results and Discussion

3.1. Compressive Strength Analysis

3.1.1. Influence of Solid Sodium Silicate

The effect of SSS on the compressive strength of alkali-activated slag specimens is shown in Figure 1a. The compressive strength of specimen X-1 (activated only by sodium hydroxide) cured for 3 days was only 12.7 MPa. When the curing time was prolonged to 28 days, the compressive strength only increased to 23.6 MPa, which was significantly lower than that of cement mortars at the same age (about 40–50 MPa) [18]. Moreover, with the increase in curing age, the growth range of compressive strength for specimen X-1 was limited. This indicates that the compressive strength of alkali-activated slag specimens activated only by sodium hydroxide was inadequate, which also shows that alkali-activated slag materials do not give full play to their performance advantages [19].

When SSS was added, the compressive strength of specimen X-2 (22.5 g, 5%) increased to 16.8 MPa, 28.4 MPa, and 33.1 MPa when cured for 3 days, 28 days, and 60 days, respectively. These values were 32.2%, 20.8%, and 23.5% higher than the corresponding strengths of specimen X-1. The addition of SSS markedly enhanced the compressive strength, and the co-activation effect of SSS and sodium hydroxide was significantly better than that of specimen X-1. The addition of SSS can provide a large amount of active silicon for alkali-activated materials, which is an important part of hydrated calcium silicate and calcium aluminosilicate gel. Therefore, the addition of SSS promoted the formation of polymerization products, which significantly improved the compressive strength of the specimen [20].
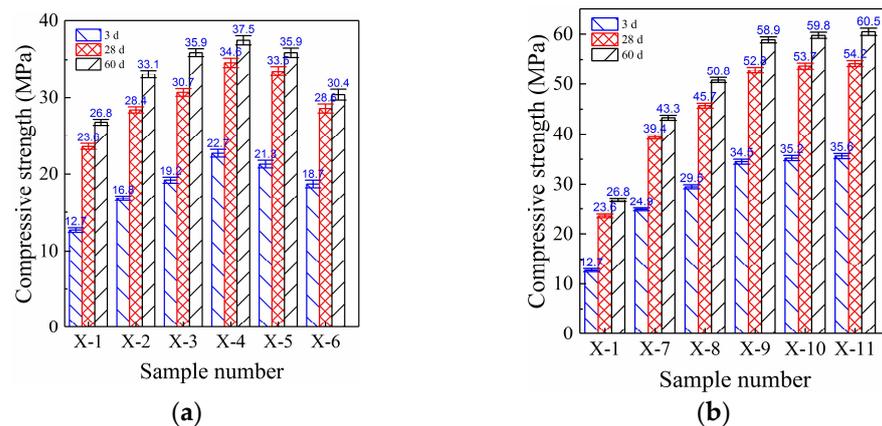
Figure 1. Regulation effect of sodium silicate on compressive strength (**a**) Solid sodium silicate excitation (**b**) Liquid sodium silicate excitation.

The compressive strength of specimens X-3 to X-6 continued to increase significantly with increases in SSS content. When SSS content increased to 45 g (10%), the compressive strength of specimen X-4 reached 22.7 MPa, 34.6 MPa, and 37.5 MPa when cured for 3 days, 28 days, and 60 days, respectively. These values were 35.1%, 21.8%, and 13.3% higher than those of specimen X-2, respectively, reaching the best effect of SSS reinforcement. An increase in SSS content can continuously improve the compressive strength. SSS is mainly composed of silica and sodium oxide. After mixing with water, silicon and sodium can be released into the reaction environment after dissolving. With the increase in SSS content, the amount of silicon was also significantly increased. This further improved the polymerization efficiency and promoted the formation of polymerization products, thus significantly enhancing the compressive strength [21].

However, when SSS content increased to 56.25 g (12.5%), the compressive strength of specimen X-5 reached 21.3 MPa, 33.5 MPa, and 35.9 MPa when cured for 3 days, 28 days, and 60 days, which were 6.2%, 3.2%, and 4.3% lower than those of specimen X-4, respectively. Moreover, when SSS content increased to 67.5 g (15%), the compressive strength of specimen X-6 further decreased to 18.7 MPa, 28.6 MPa, and 30.4 MPa when cured for 3 days, 28 days, and 60 days, which were 12.2%, 14.6%, and 15.3% lower than those of specimen X-5, respectively. When SSS content exceeded 45 g (more than 10%), the compressive strength decreased with the increase in SSS content, and the reduction range increased significantly with the gradual increase in content. The active silicon in SSS must be dissolved into the reaction solution before it can play an enhancement role. Hence, when SSS content was more than 10%, the excess SSS could not dissolve and further improve the active silicon content in the reaction solution. Instead, it was mostly deposited in the specimen, affecting the compactness of the structure, and finally, reducing the compressive strength [22]. Therefore, with the increase in SSS content, the enhancement effect of compressive strength increased first and then decreased; 45 g (10%) of SSS was found to be the optimum content. The mechanism of strength decrease caused by excessive addition of SSS was further investigated through XRD and optical microscope analyses, which will be discussed in later sections.

3.1.2. Influence of Liquid Sodium Silicate

The effect of LSS on the compressive strength of specimens is shown in Figure 1b. The compressive strength of specimen X-7 (65 g, 5% LSS) reached 24.9 MPa, 39.4 MPa, and 43.3 MPa when cured for 3 days, 28 days, and 60 days, respectively. These values were 48.2%, 38.7%, and 30.8% higher than those of specimen X-2 (mixed with 5% SSS). The addition of LSS can significantly improve the compressive strength. More importantly, the enhancement effect of LSS was significantly better than that of SSS. Silicon in LSS is in liquid form, and LSS is prepared by autoclave reaction at 2–3 atmospheres. The solubility of

silicon in LSS is significantly higher compared to SSS. Therefore, under the condition of the same dosage, liquid silicon in LSS participates in the reaction more quickly and efficiently, further enhancing the efficiency of the reaction, while SSS cannot play such a role. This is the reason for the superior enhancement effect of LSS [23].

The compressive strength of alkali-activated specimens X-8 to X-11 was further enhanced with the increase in LSS content and the enhancement range was still large. When LSS content increased to 128 g (10%), the compressive strength of specimen X-9 reached 34.5 MPa (cured for 3 days), 52.8 MPa (cured for 3 days), and 58.9 MPa (cured for 3 days), which were 16.9%, 15.5%, and 15.9% higher, respectively, than those of specimen X-8 (mixed with 7.5%, 96 g LSS). With a continuous increase in LSS content, the compressive strength continued to improve significantly, and the range of increase was still large. Since the silicon contained in LSS exists in liquid form, it does not need to be released through dissolution, as does SSS [24]. Therefore, increasing the content of LSS can continuously aid in increasing silicon, improving the polymerization rate, accelerating the fusion of active substances such as calcium, silicon, and aluminum, and can significantly improve the mechanical properties of the specimen.

However, the compressive strength of specimens X-10 (160 g, 12.5%) and X-11 (193 g, 15%) increased slowly with a further increase in LSS content. This was completely different from the strengthening mechanism of SSS (significantly reduced). The compressive strength of specimen X-10 reached 35.2 MPa (cured for 3 days), 53.7 MPa (cured for 28 days), and 59.8 MPa (cured for 60 days). These values were only 2%, 1.7%, and 1.5% higher than those of specimen X-9, respectively. The increase amount was extremely insignificant. The compressive strength of specimen X-11 reached 35.6 MPa (cured for 3 days), 54.2 MPa (cured for 28 days), and 60.5 MPa (cured for 60 days). These values were only 1.1%, 0.9%, and 1.2% higher than those of specimen X-10, respectively, indicating that the growth rate was further reduced.

3.2. Analysis of Condensation Behavior

3.2.1. Influence of Solid Sodium Silicate

The effect of sodium silicate on the condensation behavior of slag alkali activated specimens is shown in Figure 2. When only sodium hydroxide was used as activator, the initial setting time (IST) of specimen X-1 (Figure 2a) was 116 min, while the final setting time (FST) reached 203 min. Under the strong alkali excitation environment established by sodium hydroxide, the active calcium, silicon and aluminum in slag were depolymerized, dissolved into the reaction solution and re-polycondensated to form new polymerization products. This is the mechanism responsible for the condensation and hardening of specimen X-1. However, compared with Portland cement, the IST of specimen X-1 was longer, but the FST was significantly shorter. Moreover, the time interval between initial and final setting times (defined as TIST) of specimen X-1 was only 87 min, which was obviously lower than that of cement. Only under the condition of sodium hydroxide excitation, the initial polymerization rate of alkali activated specimen was lower than cement hydration rate, but the formation rate and amount of polymerization products were significantly faster compared to cement hydration products [25].

When 22.5 g (5%) of SSS was added, the IST and FST of specimen X-2 (Figure 2a) were shortened to 82 min and 134 min, respectively, which were 29.3% and 34.0% lower than those of specimen X-1. Moreover, the TIST in specimen X-2 was shortened to 52 min, which was 40.2% lower than that of specimen X-1. Addition of SSS significantly speeded up the polymerization rate of slag alkali activated materials, accelerated the formation of reaction products, led to the accelerated condensation of slag alkali activated materials, and finally shortened the IST and FST. This was also the reason for the increase in compressive strength after the addition of SSS.

When the content of SSS increased to 45 g (10%), the IST and FST of specimen X-4 (Figure 2a) were shortened to 39 min and 54 min, respectively, which were 33.9% and 41.3% lower compared to specimen X-3. Moreover, the TIST of specimen X-4 was only 15 min,

which was 45.5% lower compared to specimen X-3. With increase in the content of SSS, the IST and FST continued to shorten and the decreasing range gradually expanded. With increase in SSS content, the amount of active silicon provided for the polymerization reaction was significantly increased. This was conducive to the rapid formation of polymerization products and to accelerate the condensation of specimens [26]. Moreover, SSS can release active silicon to the polymerization reaction through the dissolution process, while the active silicon provided by slag must be through the depolymerization and dissolution process. Considering the supply efficiency of active silicon, SSS was obviously better than slag, which was also the reason for the accelerated condensation with the increase in SSS content.
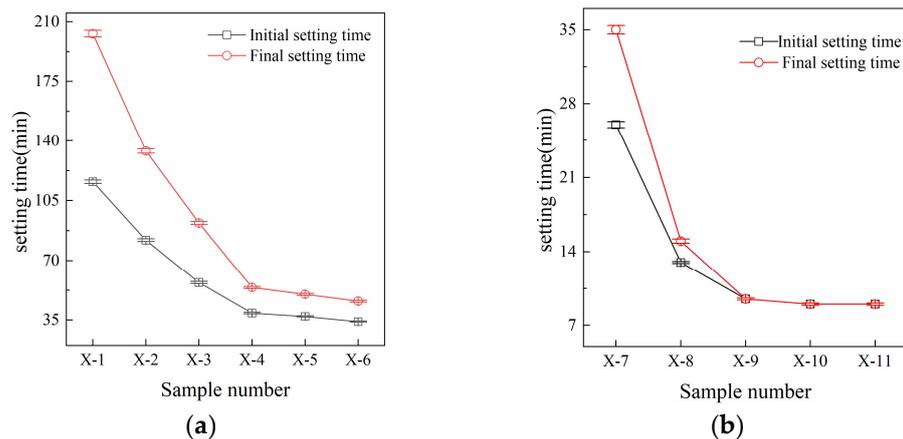

Figure 2. Regulation effect of sodium silicate on condensation behavior (**a**) Solid sodium silicate impact (**b**) Liquid sodium silicate impact.

However, the IST and FST of specimen X-5 (56.25 g, 12.5% SSS, Figure 2a) were shortened to 36 min and 49 min, which were only 7.7% and 11.1% lower compared to specimen X-4. Moreover, the TIST was 13 min in specimen X-5, which was 13.3% lower than that of specimen X-4. Furthermore, when SSS content exceeded 45 g, the setting time of specimen X-5 was further shortened, but the reduction range was significantly decreased.

When SSS content increased to 67.5 g (15%), the IST and FST of specimen X-6 (Figure 2a) further shortened to 34 min and 46 min, only 5.6% and 6.1% lower compared to specimen X-5. Moreover, the TIST was 12 min, which was only 7.7% lower than that of specimen X-5. Compared with specimen X-5, the reduction of setting time was significantly decreased. Owing to the limited solubility of SSS, the increase in SSS content could not enhance the content of soluble active silicon in the reaction solution once its content exceeded the solubility [27]. Therefore, the polymerization rate cannot improve further. This is the reason why the setting time of specimens X-5 and X-6 was not significantly shortened. On the contrary, the large amount of SSS that does not participate in the polymerization reaction can condense in the specimens, which will hinder the development of compressive strength (this will be further described in the optical microscope analysis section).

3.2.2. Influence of Liquid Sodium Silicate

With the addition of LSS, the condensation behavior of specimens X-7 to X-11 changed markedly. When LSS content reached 65 g (5%), the IST and FST of specimen X-7 (Figure 2b) were shortened to 26 min and 35 min, respectively, which were 68.3% and 73.9% lower compared to specimen X-2 (mixed with 22.5 g, 5% SSS). Moreover, the TIST of specimen X-7 was only 15 min, 71.2% lower than that of specimen X-2. Under the same amount of sodium silicate but different types, the condensation rate of specimen X-7 (liquid) was significantly faster than that of specimen X-2 (solid), and its mechanical property was also significantly higher than that of specimen X-2. LSS evidently showed better excitation effect than SSS. Silicon in LSS exists completely in liquid active form, which can undergo direct polycondensation with active calcium, aluminum, etc. However, silicon in SSS

exists completely in solid form, which must be dissolved in the reaction solution before it has reactivity. Moreover, LSS is formed by reaction in a high-pressure steamer under 0.6–1.0 MPa steam, so the solubility of silicon is significantly higher than SSS under normal pressure [28]. Therefore, LSS is obviously superior to SSS in terms of the supply mode and the content of active silicon, which explains the faster condensation rate of specimen X-8 compared to specimen X-2 under the same dosage.

　　With increase in LSS content, the setting time of specimens was further reduced. When LSS content increased to 128 g (10%), the IST and FST of specimen X-9 (Figure 2b) were both shortened to 9 min, which was only 30.8% and 40% lower than that of specimen X-8. At the same time, the initial and final setting of specimen X-9 were reached. Increasing the LSS content can further accelerate the reaction rate, promote the formation of polymerization products. Hence, the setting time was further accelerated and the compressive strength continuously increased [29]. However, when LSS content continued to increase, the IST and FST of specimens X-10 and X-11 (Figure 2b) both remained at 9 min, which was no longer shortened compared to specimen X-9. When the LSS content exceeded 128 g, the condensation of specimens was not further accelerated. This indicates that the silicon increasing effect of LSS reached the upper limit and could not further accelerate the polymerization rate. The optimum content of LSS was determined to be 128 g (10%).

3.3. XRD Analysis

3.3.1. Effect of Sodium Hydroxide

　　The crystal structure analysis of paste specimens X-1, X-2, X-4, X-7, X-9 and X-11 is shown in Figure 3. When only sodium hydroxide was used as activator, the characteristic peaks of quartz with high intensity appeared at 20.9°, 26.6° and 60.0° in specimen X-1 (Figure 3a), indicating that there was a large amount of silica in specimen X-1. Weak characteristic peaks of tobermorite at 29.9°, 35.7° and 39.8°, weak characteristic peaks of hillebrandite at 30.4°, 32.7° and 37.3°, and weak characteristic peaks of gehlenite at 31.1°, 37.4° and 47.1° also appeared in specimen X-1. Tobermorite, hillebrandite and gehlenite are types of calcium silicate and calcium aluminosilicate minerals. They are generally considered as hydrated calcium silicate (C-S-H) and hydrated calcium aluminosilicate (C-A-S-H) gels. They are the main polymerization products of alkali activated materials and the main driving force for the development of mechanical property [30]. However, the intensity of their characteristic peaks was weak, indicating that the crystallinity of these minerals was poor and that they were formed in small amounts. This implied that the polymerization reaction was not sufficient, which also explained the limited compressive strength of specimen X-1.

Figure 3. Crystal structure analysis of alkali-activated slag samples (**a**) Solid sodium silicate impact (**b**) Liquid sodium silicate impact.

3.3.2. Influence of Solid Sodium Silicate

The diffraction pattern of specimen X-2 (Figure 3a), addition of 22.5 g SSS, 5%) significantly improved. The intensity of quartz characteristic peak at 26.6° in specimen X-2 was markedly reduced (compared with specimen X-1), indicating that the addition of SSS significantly improved the degree of active silicon participating in polymerization. This promoted the transformation of active silicon to calcium silicate and calcium aluminosilicate, which was the reason for the obvious decrease in intensity of quartz characteristic peak. Moreover, the characteristic peaks of tobermorite at 29.8° and 35.7° and the characteristic peaks of hillebrandite at 30.4° and 32.7° showed higher intensity in specimen X-2 compared to specimen X-1. However, the characteristic peaks of gehlenite (31.1°, 37.4° and 47.1°) in specimen X-2 were not higher compared to specimen X-1. The formation amount of hydrated calcium silicate gel in specimen X-2 increased significantly, but the formation amount of hydrated calcium aluminosilicate gel did not increase. The addition of SSS contributed to the formation of high strength polymerization products, which explains why the mechanical property increased and the setting time significantly shortened [31].

With increase in SSS amount, the diffraction pattern of specimen X-4 (Figure 3a 45 g, 10%) further improved. Compared with specimen X-2, the intensity of quartz characteristic peaks near 20.9° and 26.6° in specimen X-4 further reduced. Moreover, the characteristic peaks representing tobermorite (29.9° and 35.6°) and hillebrandite (30.4° and 32.7°) in specimen X-4 were significantly improved. The crystallinity of hydrated calcium silicate in specimen X-4 was improved, and its formation amount was increased. Most importantly, the intensity of the three characteristic peaks (31.1°, 37.4° and 47.1°) representing gehlenite in specimen X-4 was also significantly improved. The crystallinity of hydrated calcium aluminosilicate in specimen X-4 was also improved, and its formation amount was increased. Therefore, the increase in SSS content not only promoted the formation of hydrated calcium silicate, but also promoted the formation of hydrated calcium silicoaluminate, which accelerated the setting of the specimen and benefitted the development of strength [32].

3.3.3. Influence of Liquid Sodium Silicate

With addition of LSS, the diffraction pattern of specimen X-7 (Figure 3b, 65 g, 5% liquid) further changed. Compared with specimen X-2 (22.5 g, 5% solid), the intensity of quartz characteristic peaks near 20.9°, 26.6° and 60.0° in specimen X-7 did not change significantly, but the characteristic peaks of tobermorite (29.9°, 35.7° and 39.8°) and hillebrandite (30.4°, 34.7° and 37.3°) were significantly improved, which were even higher than in specimen X-4 (45 g, 10% solid). Moreover, new characteristic peaks at 32.5° (tobermorite) and 34.2° (hillebrandite) also appeared in specimen X-7, which did not appear in specimens X-2 and X-4. This indicated that both crystallinity and formation amount of tobermorite and hillebrandite were further increased, and the degree of polymerization and reaction rate were improved to varying degrees. Therefore, the excitation effect of LSS was obviously better than that of SSS [33]. Furthermore, the intensities of the three characteristic peaks at 31.1°, 37.4° and 47.2° (gehlenite) in specimen X-7 also increased significantly compared with specimen X-2 and were slightly higher than those of specimen X-4, indicating that the formation amount of gehlenite also increased in specimen X-7.

With increase in LSS amount, the diffraction pattern of specimen X-9 (Figure 3b, 128 g, 10%, liquid) was further improved. Compared with specimen X-7 (65 g, 5% liquid), the characteristic peaks of tobermorite (30.1°, 32.5°, 35.7° and 39.8°) and hillebrandite (30.4°, 32.1°, 34.7° and 37.3°) in specimen X-9 were significantly improved. Moreover, the intensities of the three characteristic peaks representing gehlenite (31.1°, 37.4° and 47.2°) in specimen X-9 also further increased, and new characteristic peaks of gehlenite appeared at 23.9° and 52.1°, which did not appear in specimen X-7. Increasing the content of LSS increased the formation of tobermorite, hillebrandite and gehlenite, which in turn further promoted the development of compressive strength and accelerated the setting of specimens [34].

However, the characteristic peaks of tobermorite, hillebrandite and gehlenite in specimen X-11 (Figure 3b, 193 g, 15% liquid) did not increase compared with specimen X-9 (128 g, 10%, liquid). This indicates that the crystallinity and formation amount of tobermorite, hillebrandite and gehlenite cannot be further improved by continuously increasing LSS content [35]. This also explains why the compressive strength of specimens X-10 and X-11 did not continue to increase significantly and the setting time did not further shorten with the continuous increase in content of LSS. This is because the addition of LSS can only improve the active silicon in the reaction environment. However, the formation of hydrated calcium silicate and hydrated calcium silicoaluminate still requires a large amount of active calcium to participate in the reaction. The active calcium only comes from slag, and the content of slag remains unchanged. Therefore, the content of active calcium remained unchanged. Consequently, even if the LSS increased continuously, the polymerization product cannot be formed [36]. This explains why the compressive strength of specimens X-10 and X-11 did not increase significantly and the setting time did not shorten.

3.4. Optical Microscope Analysis

3.4.1. Effect of Sodium Hydroxide on Microstructure

The microstructure of specimen X-1 (200 times magnification) is shown in Figure 4a. When only sodium hydroxide was used as activator, there were many internal structural defects in specimen X-1, and several micron and millimeter sized pores and cracks were disorderly distributed. Moreover, the bonding between particles was not firm enough, and free scattered particles that do not participate in the reaction were dispersed in the specimen. This shows that the degree of polymerization of specimen X-1 was not high, and the formation of polymerization products was insufficient, which was also the reason for the limited compressive strength of specimen X-1.
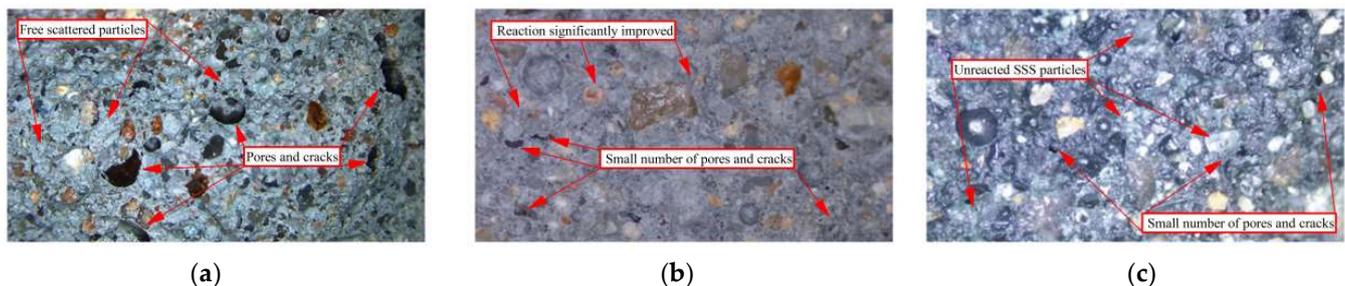

(**a**)　　　　　　　　　　　　　　　(**b**)　　　　　　　　　　　　　　　(**c**)

Figure 4. Effect of solid sodium silicate content on microstructure of alkali-activated slag samples (×200). (**a**) Sample X-1 (**b**) Sample X-4 (**c**) Sample X-6.

3.4.2. Effect of Solid Sodium Silicate on Microstructure

When the content of SSS reached 45 g (10%), the microstructure of the specimen X-4 showed a significant improvement. As seen from Figure 4b, the interior of specimen X-4 was relatively dense, the microstructure integrity was good, and the defects such as pores and cracks were significantly reduced (compared with specimen X-1). Moreover, the bonding between particles was relatively tight, and the particles not participating in the polymerization reaction were significantly reduced. Therefore, increase in SSS content significantly improved the microstructure [37]. This led to the significant increase in the mechanical property and accelerated condensation.

The microstructure of specimen X-6 with SSS content of 67.5 g (15%) is shown in Figure 4c. Compared with specimen X-4 (45 g, 10%), the internal structure of specimen X-6 was still relatively dense and the defects such as pores and cracks did not grow further. However, a large number of undissolved SSS particles were deposited in specimen X-6, while SSS particles in specimen X-4 completely dissolved and participated in the reaction. When the content of SSS reached 45 g (10%), the polymerization reached the limit, and the reaction solution could not absorb or dissolve any more SSS. However, further increase in

the content of SSS could not improve the dissolution. Moreover, the large amount of sodium silicate that did not participate in the polymerization reaction crystallized in specimen X-6 and remained in the specimen [38]. This had an adverse impact on the compactness and strength development of microstructure, as well as an extremely adverse impact on the development of the compressive strength of the specimen. This is the main reason why the compressive strength of specimens X-5 and X-6 showed no significant increase compared with specimen X-4 and setting time was not further shortened with continuous increase in SSS content.

4. Conclusions

In this study, slag-activated materials were prepared using SSS and LSS as activators respectively. XRF was carried out to determine the content and reactivity of various elements in slag. The compressive strength of the developed composites was evaluated at different ages. Moreover, the effects of different types and contents of sodium silicate on the formation of mineral crystals in slag alkali activated samples were further analyzed by XRD.

(1) The addition of SSS and LSS both significantly increased the content of silicon, promoted the formation of products, accelerated the reaction rate, significantly improved the compressive strength (maximum increase up to 123.7%) and greatly shortened the IST and FST (fastest IST was 9 min). The enhancement effect of LSS was markedly better than that of SSS.

(2) When SSS content increased from 5% to 15%, the compressive strength first increased to 34.6 MPa and then decreased to 28.6 MPa. The dosage of 45 g (10%) was the optimum content of SSS. Moreover, the IST and FST decreased significantly and then tended to stabilize, and the shortening range was gradually reduced.

(3) When LSS content increased from 5% to 15%, the compressive strength first increased to 52.8 MPa and then tended to be stable. The optimum content was found to be 128 g (10%). Moreover, the IST and FST were significantly shortened and then tended to stabilize once LSS was added.

Author Contributions: Validation, Y.C.; formal analysis, B.W.; investigation, S.Z.; resources, J.F.; data curation, Q.W.; writing—original draft preparation, G.H.; writing—review and editing, M.L. All authors have read and agreed to the published version of the manuscript.

Conflicts of Interest: The authors declare no conflict of interest.

References

1. Provis, J.L.; Palomo, A.; Shi, C. Advances in understanding alkali-activated materials. *Cem. Concr. Res.* **2015**, *78*, 110–125. [CrossRef]
2. Luukkonen, T.; Abdollahnejad, Z.; Yliniemi, J.; Kinnunen, P.; Illikainen, M. One-part alkali-activated materials: A review. *Cem. Concr. Res.* **2018**, *103*, 21–34. [CrossRef]
3. Huang, G.; Ji, Y.; Li, J.; Hou, Z.; Jin, C. Use of slaked lime and Portland cement to improve the resistance of MSWI bottom ash-GBFS geopolymer concrete against carbonation. *Constr. Build. Mater.* **2018**, *166*, 290–300. [CrossRef]
4. Hanjitsuwan, S.; Hunpratub, S.; Thongbai, P.; Maensiri, S.; Sata, V.; Chindaprasirt, P. Effects of NaOH concentrations on physical and electrical properties of high calcium fly ash geopolymer paste. *Cem. Concr. Compos.* **2014**, *45*, 9–14. [CrossRef]
5. Huang, G.; Ji, Y.; Li, J.; Hou, Z.; Dong, Z. Improving strength of calcinated coal gangue geopolymer mortars via increasing calcium content. *Constr. Build. Mater.* **2018**, *166*, 760–768. [CrossRef]
6. Huang, G.; Li, D.; Cui, Y.; Feng, J.; Gao, Q.; Lu, T.; Zhang, Y.; Zhu, J. Compressive Strength Enhancement in Early Age Acid Activated Mortars: Mechanical Properties and Analysis. *Crystals* **2022**, *12*, 804. [CrossRef]
7. Tuyan, M.; Andiç-Çakir, Ö.; Ramyar, K. Effect of alkali activator concentration and curing condition on strength and microstructure of waste clay brick powder-based geopolymer. *Compos. Part B Eng.* **2018**, *135*, 242–252. [CrossRef]

8. Bernal, S.A.; Mejía de Gutiérrez, R.; Pedraza, A.L.; Provis, J.L.; Rodriguez, E.D.; Delvasto, S. Effect of binder content on the performance of alkali-activated slag concretes. *Cem. Concr. Res.* **2011**, *41*, 1–8. [CrossRef]

9. Nicolas, R.S.; Bernal, S.A.; Mejía de Gutiérrez, R.; van Deventer, J.S.J.; Provis, J.L. Distinctive microstructural features of aged sodium silicate-activated slag concretes. *Cem. Concr. Res.* **2014**, *65*, 41–51. [CrossRef]

10. Sun, B.; Ye, G.; De Schutter, G. A review: Reaction mechanism and strength of slag and fly ash-based alkali-activated materials. *Constr. Build. Mater.* **2022**, *326*, 126843. [CrossRef]

11. Abdila, S.R.; Abdullah, M.M.A.B.; Ahmad, R.; Nergis, D.D.B.; Rahim, S.Z.A.; Omar, M.F.; Sandu, A.V.; Vizureanu, P.; Syafwandi, S. Potential of Soil Stabilization Using Ground Granulated Blast Furnace Slag (GGBFS) and Fly Ash via Geopolymerization Method: A Review. *Materials* **2022**, *15*, 375. [CrossRef] [PubMed]

12. Ramli, M.I.I.; Salleh, M.A.A.M.; Abdullah, M.M.A.B.; Aziz, I.H.; Ying, T.C.; Shahedan, N.F.; Kockelmann, W.; Fedrigo, A.; Sandu, A.V.; Vizureanu, P.; et al. The Influence of Sintering Temperature on the Pore Structure of an Alkali-Activated Kaolin-Based Geopolymer Ceramic. *Materials* **2022**, *15*, 2667. [CrossRef]

13. Huang, G.; Ji, Y.; Li, J.; Zhang, L.; Liu, X.; Liu, B. Effect of activated silica on polymerization mechanism and strength development of MSWI bottom ash alkali-activated mortars. *Constr. Build. Mater.* **2019**, *201*, 90–99. [CrossRef]

14. Cristelo, N.; Tavares, P.; Lucas, E.; Miranda, T.; Oliveira, D. Quantitative and qualitative assessment of the amorphous phase of a Class F fly ash dissolved during alkali activation reactions-effect of mechanical activation, solution concentration and temperature. *Compos. Part B Eng.* **2016**, *103*, 1–14. [CrossRef]

15. *GB/T 18046-2017*; Granulated Blast Furnace Slag Powder Used for Cement, Mortar and Concrete. AQSIQ: Beijing, China, 2017.

16. *GB/T 17671-2021*; Method of Testing Cements—Determination of Strength. AQSIQ: Beijing, China, 2021.

17. *GB/T 1346-2011*; Test Methods for Water Requirement of Normal Consistency, Setting Time and Soundness of the Portland Cement. AQSIQ: Beijing, China, 2011.

18. Huang, G.; Yang, K.; Sun, Y.; Lu, Z.; Zhang, X.; Zuo, L.; Feng, Y.; Qian, R.; Qi, Y.; Ji, Y.; et al. Influence of NaOH content on the alkali conversion mechanism in MSWI bottom ash alkali-activated mortars. *Constr. Build. Mater.* **2020**, *248*, 118582. [CrossRef]

19. Bergold, S.; Goetz-Neunhoeffer, F.; Neubauer, J. Interaction of silicate and aluminate reaction in a synthetic cement system: Implications for the process of alite hydration. *Cem. Concr. Res.* **2017**, *93*, 32–44. [CrossRef]

20. Huang, G.; Ji, Y.; Zhang, L.; Li, J.; Hou, Z. The influence of curing methods on the strength of MSWI bottom ash-based alkali-activated mortars: The role of leaching of OH$-$and free alkali. *Constr. Build. Mater.* **2018**, *186*, 978–985. [CrossRef]

21. Huang, G.; Li, Y.; Zhang, Y.; Zhu, J.; Li, D.; Wang, B. Effect of Sodium Hydroxide, Liquid Sodium Silicate, Calcium Hydroxide, and Slag on the Mechanical Properties and Mineral Crystal Structure Evolution of Polymer Materials. *Crystals* **2021**, *11*, 1586. [CrossRef]

22. Li, C.; Sun, H.; Li, L. A review: The comparison between alkali-activated slag (Si+Ca) and metakaolin (Si+Al) cements. *Cem. Concr. Res.* **2010**, *40*, 1341–1349. [CrossRef]

23. Huang, G.; Yuan, L.; Ji, Y.; Liu, B.; Xu, Z. Cooperative action and compatibility between Portland cement and MSWI bottom ash alkali-activated double gel system materials. *Constr. Build. Mater.* **2019**, *209*, 445–453. [CrossRef]

24. Ahmari, S.; Zhang, L.; Zhang, J. Effects of activator type/concentration and curing temperature on alkali-activated binder based on copper mine tailings. *J. Mater. Sci.* **2012**, *47*, 5933–5945. [CrossRef]

25. Haha, M.B.; Saout, G.L.; Winnefeld, F.; Lothenbach, B. Influence of activator type on hydration kinetics, hydrate assemblage and microstructural development of alkali activated blast-furnace slags. *Cem. Concr. Res.* **2011**, *41*, 301–310. [CrossRef]

26. Angulo-Ramírez, D.E.; Mejía de Gutiérrez, R.; Puertas, F. Alkali-activated Portland blast-furnace slag cement: Mechanical properties and hydration. *Constr. Build. Mater.* **2017**, *140*, 119–128. [CrossRef]

27. Jin, L.; Huang, G.; Li, Y.; Zhang, X.; Ji, Y.; Xu, Z. Positive Influence of Liquid Sodium Silicate on the Setting Time, Polymerization, and Strength Development Mechanism of MSWI Bottom Ash Alkali-Activated Mortars. *Materials* **2021**, *14*, 1927. [CrossRef]

28. Gonçalves, M.; Vilarinho, I.S.; Capela, M.; Caetano, A.; Novais, R.M.; Labrincha, J.A.; Seabra, M.P. Waste-Based One-Part Alkali Activated Materials. *Materials* **2021**, *14*, 2911. [CrossRef]

29. Shi, Z.; Shi, C.; Zhang, J.; Wan, S.; Zhang, Z.; Ou, Z. Alkali-silica reaction in waterglass-activated slag mortars incorporating fly ash and metakaolin. *Cem. Concr. Res.* **2018**, *108*, 10–19. [CrossRef]

30. Li, Y.; Zhang, H.; Huang, G.; Cui, Y.; Feng, J.; Zhang, Y.; Li, D.; Zhu, J. Preparation and Properties of Municipal Solid Waste Incineration Alkali-Activated Lightweight Materials through Spontaneous Bubbles. *Polymers* **2022**, *14*, 2222. [CrossRef]

31. Bernal, S.A.; Provis, J.L.; Rose, V.; Mejía de Gutierrez, R. Evolution of binder structure in sodium silicate-activated slag-metakaolin blends. *Cem. Concr. Compos.* **2011**, *33*, 46–54. [CrossRef]

32. Bernal, S.A.; Nicolas, R.S.; Myers, R.J.; Mejía de Gutierrez, R.; Puertas, F.; van Deventer, J.S.J.; Provis, J.L. MgO content of slag controls phase evolution and structural changes induced by accelerated carbonation in alkali-activated binders. *Cem. Concr. Res.* **2014**, *57*, 33–43. [CrossRef]

33. Huang, G.; Zhu, J.; Zhang, Y.; Li, D.; Wang, B.; Li, M.; Jin, L.; Gong, J. The Effect of Slag on the Mechanical Properties of Coralline-Activated Materials and the Formation and Transformation of Mineral Crystals. *Crystals* **2022**, *12*, 470. [CrossRef]

34. Huang, G.; Yang, K.; Chen, L.; Lu, Z.; Sun, Y.; Zhang, X.; Feng, Y.; Ji, Y.; Xu, Z. Use of pretreatment to prevent expansion and foaming in high-performance MSWI bottom ash alkali-activated mortars. *Constr. Build. Mater.* **2020**, *245*, 118471. [CrossRef]

35. Huang, G.; Ji, Y.; Zhang, L.; Li, J.; Hou, Z. Advances in Understanding and Analyzing the Anti-diffusion Phenomenon in Complete Carbonization Zone of MSWI Bottom Ash-based Alkali-activated Concrete. *Constr. Build. Mater.* **2018**, *186*, 1072–1081. [CrossRef]

36. Huang, G.; Ji, Y.; Zhang, L.; Hou, Z.; Zhang, L.; Wu, S. Influence of calcium content on structure and strength of MSWI bottom ash-based geopolymer. *Mag. Concr. Res.* **2019**, *71*, 362–372. [CrossRef]

37. García-Lodeiro, I.; Fernández-Jiménez, A.; Palomo, A.; Macphee, D.E. Effect of Calcium Additions on N-A-S-H Cementitious Gels. *J. Am. Ceram. Soc.* **2010**, *93*, 1934–1940. [CrossRef]

38. Walkley, B.; Nicolas, R.S.; Sani, M.-A.; Bernal, S.A.; van Deventer, J.S.J.; Provise, J.L. Structural evolution of synthetic alkaliactivated CaO-MgO-Na$_2$O-Al$_2$O$_3$-SiO$_2$ materials is influenced by Mg content. *Cem. Concr. Res.* **2017**, *99*, 155–171. [CrossRef]